This is a preprint, the final version is subject to change, of the American Mineralogist (MSA)
Cite as Authors (Year) Title. American Mineralogist, in press.
(DOI will not work until issue is live.) DOI: http://dx.doi.org/10.2138/am-2015-4905 12/2

Surface transformations of platinum grains from Fifield, New South Wales, Australia (Revision 2)

S. Gordon Campbell[1], Frank Reith[2,3], Barbara Etschmann[4,5], Joël Brugger[4,6], Gema Martinez-Criado[7], Robert A. Gordon[8] and Gordon Southam[9*]

[1]Department of Earth Sciences, The University of Western Ontario, London, ON, N6A 5B7, Canada.

[2]Centre for Tectonics, Resources and Exploration, School of Earth and Environmental Sciences, The University of Adelaide, North Terrace, SA 5000, Australia.

[3]CSIRO Land and Water, Environmental Biogeochemistry, PMB2, Glen Osmond, SA 5064, Australia.

[4]Division of Mineralogy, South Australian Museum, Adelaide, SA 5000, Australia.

[5]School of Chemical Engineering, The University of Adelaide, North Terrace, Adelaide, SA 5005, Australia.

[6]School of Geosciences, Monash University, Clayton, VIC 3800, Australia.

[7]Experiments Division, European Synchrotron Radiation Facility, 38043 Grenoble, France.

[8]PNCSRF, Advanced Photon Source, Argonne, IL, USA 60439.

[9]School of Earth Sciences, The University of Queensland, St Lucia, QLD 4072, Australia.

*Corresponding author: g.southam@uq.edu.au

Abstract

A growing literature is demonstrating that platinum (Pt) is transformed under surface conditions; yet (bio)geochemical processes at the nugget-soil-solution interface are incompletely understood. The reactivity of Pt exposed to Earth-surface weathering conditions, highlighted by this study, may improve our ability to track its movement in natural systems, e.g., focusing on nanoparticles as a strategy for searching for new, undiscovered sources of this precious metal. To study dissolution/re-precipitation processes of Pt and associated elements, grains of Pt-Fe alloy were

collected from a soil placer deposit at the Fifield Pt-field, Australia. Optical- and electron-microscopy revealed morphologies indicative of physical transport as well as chemical weathering. Dissolution 'pits', cavities, striations, colloidal nano-particles and aggregates of secondary Pt platelets as well as acicular, iron (Fe) hydroxide coatings were observed. FIB-SEM-(EBSD) combined with S-µ-XRF of a sectioned grain showed a fine layer of up to 5 µm thick composed of refined, aggregates of 0.2 to 2 µm-sized crystalline secondary Pt overlying more coarsely crystalline Pt-Fe-alloy of primary magmatic origin. These results confirm that Pt is affected by geochemical transformations in supergene environments; structural and chemical signatures of grains surfaces, rims and cores are linked to the grains' primary and secondary (trans)formational histories; and Pt mobility can occur under Earth surface conditions. Intuitively, this nanophase-Pt can disperse much further from primary sources of ore than previously thought. This considerable mineral reactivity demonstrates that the formation and/or release of Pt nanoparticles needs to be measured and incorporated into exploration geochemistry programs.

Keywords: platinum, weathering, Fifield Pt-Province, secondary mineralization, Australia

Introduction

Platinum is a highly prized noble metal; its resistance to oxidation and corrosion in combination with its unique surface properties makes it an important catalyst in industrial processes and automobile catalytic converters (MacDonald 1987). With ca. 90 % of the world's production of Pt coming from the Republic of South Africa and the Russian Federation, Pt is a highly strategic resource, important to resource security (Koek et al. 2010). To enhance exploration success, a fundamental understanding of (bio)geochemical processes leading to Pt

dispersion in surface environments needs to be developed. Understanding Pt-Fe alloy weathering is one component that will improve our ability to recover Pt from soils and track its movement in nature. This could potentially lead to new, undiscovered sources of this precious metal and to an improved understanding of the cycling of industrial Pt-nanoparticles in the environment.

Schneiderhöhn and Moritz (1939) described native Pt that was entirely porous from the oxidized zone of the Merensky Reef, Bushveld Complex, Republic of South Africa that they interpreted as a dissolution feature of a pre-existing mineral, such as sperrylite or cooperite. Native Pt as rims was subsequently observed on both sperrylite (Oberthu□r et al. 2003, 2013; Melcher et al. 2005) and on cooperite (Oberthu□r 2002; Oberthu□r et al. 2004). Platinum mobility can occur in eluvial, alluvial and lateritic environments in tropical and possibly also semi-arid climates (Bowles 1986; Freyssinet et al. 2005). Under supergene conditions Pt may be oxidized, dissolved, complexed by inorganic- and organic- ligands, transported, re-precipitated and deposited, yet these processes are incompletely understood (Fuchs and Rose 1974; Bowles 1986; Hanley 2005). The reactivity of platinoids to secondary processing appears to vary based on the reactivity of the starting material. Placer Pt grains are often larger than the primary sources they are derived from (Cousins and Kinloch 1973, 1976) suggesting that secondary processes contribute to growth or aggregation of these materials. Conversely, other studies indicate that Pt-Fe alloy is susceptible to dissolution and will “shrink” in weathering environments (Cabral et al. 2007; Traoré et al. 2008). Evidence, for a biogenic contribution to the formation of the arborescent Pt–Pd nuggets, and the presence of organic matter in these grains, has recently been described (Cabral et al. 2011). This continuum of dissolution versus

growth is typically revealed using mineralogical and petrologic analyses of placer Pt-grains, highlight the opposing processes that can transform Pt-grains in natural systems.

The internal composition of eluvial and alluvial Pt-Fe alloy from the Fifield site proves a high temperature primary origin (Slansky et al. 1991); however, to better understand the weathering of Pt-Fe alloy in surficial environments, chemical characterization of mineral dissolution-precipitation processes occurring at the solid-solution interface needs to be conducted. In a recent study, Brugger et al. (2013) compared the μm-scale dispersion of Au and Pt within an extraordinary 10 mm-sized fragment of ferruginous palaeochannel material from Fifield that contained a number of native Au- and Pt-Fe alloy (based on the classification scheme of Cabri et al. 1996). While Au grains were surrounded by an abundant dusting of highly pure metallic Au particles (10 nm < secondary Au < 10 μm in diameter), which is indicative of (bio)geochemical transformations (Reith et al. 2007, 2010; Southam et al. 2009), secondary Pt was not observed in this sample. In contrast, the Pt-Fe alloy grains appeared smoother and more rounded, but also displayed signs indicative of supergene transformations, e.g., herringbone-shaped embayments, possibly pointing to the weathering-out of a more reactive material, e.g., Os-Ir alloy inclusions. However, to establish if Pt itself is mobilized and/or re-precipitated from Pt-Fe alloy in weathering environments, additional research on a larger number of these grains needs to be undertaken using targeted micro-analyses techniques. The specific focus of this study was placed on the examination of mechanical and chemical evidence for nano- and microscale surface transformations resulting the redistribution of Pt, which should be detectable using Electron microprobe mapping, (Focused Ion Beam)-Scanning Electron Microscopy-(Energy Dispersive X-ray Analysis/Electron BackScatter Diffraction) (FIB)-SEM-(EDXA/EBSD) in combination with electron X-ray emission spectroscopy: X-ray Analysis Near

Edge Structure (XANES), micro X-Ray Fluorescence (μXRF) and micro X-Ray Diffraction (μXRD).

Materials and Methods

Field Description and Sampling

The Fifield Pt-field, situated about 380 km WNW of Sydney, Australia (Figure 1), was the largest Australian producer of Pt: 650 kg of Pt and 325 kg of Au were recovered from Pleistocene gravels and recent residual soils since its discovery in 1887 (Johan et al. 1989). The Fifield Pt-field is part of the Fifield Pt-province, which contains ca. 40 Alaskan-type mafic-ultramafic intrusions (monzodiorite, gabbro-norite, hornblendite, hornblende/olivine/biotite/magnetite-clinopyroxenite, peridotite and dunite complexes). These late Ordovician to Siluro-Devonian magmatic bodies intrude into Cambro-Ordovician metasediments and, locally, Silurian and Devonian volcanics and sediments (Crawford et al. 2007; Johan et al. 1989; Slansky et al. 1991). Mineralization associated with chromite-rich layers within dunites is dominated by Pt-Fe alloy with inclusions of Os-Ir alloy, and rare inclusions of Ru, Rh and Ir sulfides (Johan et al. 1989; Slansky et al. 1991). Landscape evolution at the site commenced in the Early to Middle Devonian, and subsequent periods of weathering, laterization and fluvial erosion have continued since then. Since the Jurassic, Pt and Au grains have been concentrated into a number of paleoplacers that have been reworked throughout the Cenozoic (Teluk 2001). The grains used in this study were obtained from the soils overlying the Platina Deep Lead, which is assumed to be of early Tertiary age. While these grains are considered to be primary, a primary source of mineralization for these grains has not been determined (Slansky et al. 1991; Teluk 2001). The regolith over the Platina Lead Pt-Au

bedrock source area is a Pt-Au bearing residual soil, classified as a red podsol, with limited Fe pisolitic pebble development (Northcote 1979).

Two hundred and fifty Pt grains, representing the dominant morphotypes, were subsampled from ca. 500 g of placer Pt using a field-sterile sampling procedure described by Reith et al. (2010). Upon collection, 20 grains were immediately submerged in 2 vol. $\%_{(aq)}$ glutaraldehyde to fix any biological materials.

Micro-analyses of Pt grains

Platinum grains from the Fifield Pt Province were screened by using an optical binocular microscope equipped with a Nikon DXM1200 digital camera. Representative grains reflecting the diversity of morphologies observed in the sample were selected for micro-analytical characterization.

Ten representative grains were set in epoxy resin, polished with 1 μm diamond paste, C-coated (15 nm) and subjected to electron microprobe mapping (EPMA) using a Cameca SX51 Microprobe (Cameca, France) equipped with five wavelength dispersive spectrometers as described by Fairbrother et al. (2012). Data collection and reduction was performed with the SAMx package. Analyses were conducted at 20 kV and 19.9 nA with a 1 μm beam diameter.

To investigate possible biogenic components, the twenty glutaraldehyde-fixed grains were dehydrated using a 25, 50, 75 and 3 times 100 vol. $\%_{(aq)}$ ethanol series for 15 min each, critical point dried using a Tousimis Samdri®-PVT-3B drier, and Os-coated (5 nm; Osmium Plasma Coater Model OPC-80T - SPI Supplies). A LEO 1530 field emission gun-scanning electron microscope (FEG-SEM), a Zeiss 1540 XB, a Philips XL30-, and a Hitachi SU 6600 analytical FEG-SEM were used to produce high-resolution micrographs. An Oxford

Instruments' INCAx-sight energy dispersive spectrophotometer (EDS) on the Zeiss 1540 SEM and an Oxford Xmax Silicon Drift Detector EDS on the Hitachi SU 6600 SEM were used for element identification.

Two of the glutaraldehyde fixed grains possessing evidence of weathering and secondary minerals were analyzed at the Pacific Northwest Consortium/X-ray Science division (PNC-XSD) Sector 20 - Insertion Device beamline at the Advanced Photon Source, Argonne National Laboratory, Argonne, IL, USA. X-ray emission spectroscopy was conducted to map the element distribution on grain surfaces. X-ray emission energy reference values from Kortright and Thompson (2001) were used to determine elements present in the scans. X-ray Absorption Near Edge Structure (XANES) energy measurements were conducted at points of interest to determine the oxidation state of iron. Triplicate XANES energy measurements of the Fe-K edge were collected at each spot and compared to the inflection of an Fe-reference foil edge (7112 eV; Williams 2001). Beam energy was set to 10700 eV. Element maps and X-ray emission spectra were analyzed using National Instruments™ LabVIEW™ 2-D Scan Plot v. 4 and National Instruments™ LabVIEW™ 1-D Scan Plot v. 3. XANES data was processed by ATHENA analysis software (Ravel and Newville 2005). The Fe-K edge of the samples was compared to the Fe-K edge of the reference foil.

Three Pt grains possessing nanophase and μm-scale surface Pt were selected for detailed structural analysis of ion milled grains using a focused ion beam-secondary electron microscope (FIB-SEM; Helios NanoLab DualBeam, FEI, Netherlands). Images were collected from 3 to 15 kV, with sectioning and cleaning carried out at 30 kV and 21 nA and 20 kV and 2.8 to 0.34 nA, respectively.

Electron backscatter diffraction (EBSD) analyses were performed after milling a small, rounded Pt grain using an EDAX-TSL EBSD system fitted to a FEI Helios NanoLab platform. The sample (a FIB-sectioned Pt-grain) was rotated to face to the Hikari EBSD camera and tilted to 70° with respect to the camera. EBSD patterns were collected on milled regions at 20 kV and 2.7 nA with a working distance of ~9 mm and a step-size of 0.1 μm. OIM Data Collection (V5.2) and OIM Analysis (V4.5) were used for data collection and interpretation. This FIB-sectioned grain was also examined using S-μXRF at the ID22NI beamline - European Synchrotron Research Facility (ESRF). ID22NI is an undulator beamline with X-ray optics designed to focus the beam to nm size in pink beam mode operation. The beamline has a Si mirror at an incident angle about 2.6 mrad for high harmonic rejection. In the Kirkpatrick-Baez geometry used in this experiment, the focusing system comprises of two elliptically shaped mirrors, with a graded multilayer coating the first one, thus functioning both as monochromator and vertical focusing optics. The beam was focused to 120 nm, with an incident energy of 17500 eV. The sample was mounted on a XY-piezo-nano-positioner stage and scanned at the focal plane, while the emitted X-ray fluorescence data were measured with a single-element Si Drift detector. S-μXRF data were analyzed with GeoPIXE II (Ryan et al. 2005), using the dynamic analysis (DA) method to project quantitative elemental images from the full fluorescence spectra (Ryan 2000; Ryan et al. 2009).

Results

The morphology of the Fifield native Pt grains (based on Cabri et al. 1996 - composition > 80% Pt; determined using EDS; data not shown) ranged from subhedral to well-rounded, and included grains with and without negative crystal imprints (Figure 2 a-f). Pitting, cavities and

199 striations are common on the surfaces of many grains, and demonstrate that the 'nugget-soil-
200 solution' interface is an important site of mechanical and chemical weathering (Figures 2-5).
201 EPMA mapping of polished whole mounts (e.g., Figure 3) provided evidence for exsolution of
202 Os-Ir alloys indicative of primary material derived from differentiation of the melt; however, no
203 zones of enrichment or depletion of Pt were observed along the rims at the spatial resolution of
204 EPMA.

205 Tens of μm-scale dissolution pits and cavities were observed using FEG-SEM, some of
206 which were in-filled with organic matter and clay-sized materials (Figures 4 and 5). In fact, most
207 of the depressions in the grain surfaces that were partially coated by visible orange/red to dark
208 brown layers of Fe-hydroxides, with aluminosilicates, clay-sized minerals, and organic material
209 (Figures 2 and 4). Using FEG-SEM, acicular Fe-hydroxides were detected primarily within the
210 clay patches, but they were also directly affixed to the Pt-grain surfaces (Figures 4g and 5cd).
211 Energy-dispersive spectroscopy (Figures 4fg and 5e) and XANES spectra (Figure 5f) confirmed
212 that the acicular, Fe-bearing minerals exist in an oxidized Fe^{3+} state, and are likely oxygen-
213 bound, as indicated by the *K*-edge located approximately 13 eV up-energy shift from the Fe^0
214 standard (O'Day et al. 2004). XANES and EDS detected trace amounts of Cu and Rh in these
215 grains (Figures 4 and 5). SEM micrographs show fine-grained, 150 nm cubic Pt-Cu minerals
216 suggesting the presence of sub-micrometer tulameenite ($PtFe_{0.5}Cu_{0.5}$; based on their cubic
217 structure and chemistry, demonstrating that hydrothermal alteration of these grains has occurred
218 (see Cabri et al. 1996); no bacteria were observed on the surface of these Pt grains. An attempt
219 to extract and recover these cubic minerals using sonication was not successful; micro-XRD was
220 also unsuccessful in identifying these cubic minerals over the background isoferroplatinum
221 signal.

BSE-SEM-imaging of grain surfaces nanophase to μm-scale Pt (Figure 6) highlighted the presence of low numbers of spheroidal and elongated nanophase Pt typically ranging from 50 to 200 nm in diameter (Figure 6b). Aggregates of Pt-platelets were also observed on the surface of some grains, individual platelets were between 0.2 and 4 μm in diameter (Figure 6c). FIB-SEM showed that a zone of μ-crystalline Pt was common beneath the Fe-hydroxide with crystal sizes becoming larger towards the center of the slice (Figure 6 d-f).

EBSD analyses on the small, FIB-milled cross section demonstrated the occurrence and distribution of secondary Pt, (Figure 7a). While the core of the grain consisted of a large set of twinned crystals, consistent with a magmatic origin, a narrow layer (up to 5 μm) of microcrystalline-Pt was observed coating part of the grain (Figure 7ab). In these areas, distinctive electron backscattered patterns (EBSD) were obtained from individual crystals, down to 200 nm in size, which displayed highly variable orientations compared to adjacent crystals (Figure 7b). Synchrotron-μXRF at a spot size of 100 nm was used to assess the chemical gradient from surface to interior and provide clues to the dissolution and precipitation processes affecting Pt grains (Figure 7). Using μXRF, a quantifiable difference of Pt/Fe contents of the thin layer of finely crystalline secondary Pt compared to the primary bulk elemental composition was detected (Figure 7c-f). The fine layer of secondary Pt consisted of up to 91 wt. %, Pt concentrations in the bulk lay around 85 wt. %.

Discussion

Large-scale differences were observed in surface fracturing and pitting. This heterogeneity suggests that the grains were subjected to differing degrees of (bio)geochemical and physical weathering, e.g., abrasion. A number of fluvial and lateritic environments affected

the Fifield Pt Province throughout the Cenozoic, and the diverse morphologies characterized by this and previous work, are indicative of those conditions (Teluk 2001).

Deep weathering scars, pits and cavities demonstrate that the surfaces of Pt grains are important sites of mechanical and more importantly, geochemical weathering. Long, 'ordered' parallel scars mar the placer grain in Figures 2a and 4a, and may relate to the preferential weathering of Os-Ir alloy via exsolution from the Pt-Fe alloy (Figure 3 and 4; see Slansksy et al. 1991). SEM micrographs show delicate, 150 nm cubic Pt-Cu minerals; the focal series in Figure 4 (a-c) reveals 150 nm-sized cubic minerals embedded within the surface of the grain. The presence of these cubic minerals extending out from the surface of the Pt grain, combined with similar-sized 'pits' in the surface (Figure 4f), suggests that they were physically plucked out from the more massive Pt-Fe alloy, (presumably as the matrix dissolved) releasing sub-micrometer tulameenite ($PtFe_{0.5}Cu_{0.5}$;) into the environment. The apparent dissolution of the bulk nugget around these minerals demonstrates that weathering is not homogenous, reflecting the geological conditions of the field site, and that nanophase minerals may be left in, or transported out from the regolith or farther within alluvium.

The color of the Fe-hydroxides differed slightly between grains (Figure 2), which suggests that an array of insoluble Fe-hydroxides possessing various hydration states coat the grains; Fe-hydroxides, e.g., limonite, goethite, and Fe-oxides have been detected on Pt nuggets (Bowles 1986; Ottemann and Augusthihus 1967; Suárez et al. 2008) and that weathering conditions may vary within this deposit. More importantly, the presence of acicular Fe-hydroxides provides evidence that acidic conditions occur at the grain surface, which presents a possible mechanism for chemical dissolution of platiniferous materials (Guilbert 1986; Sillitoe 2005). The oxidation of Fe promotes the formation of acid through subsequent hydrolysis of

268 water, which can alter the local chemical conditions (see Dockrey et al., 2014), forming acid,
269 which can enhance Pt solubilization (Sillitoe 2005); in particular, the precipitation of acicular Fe-
270 hydroxides immediately on grain surfaces (Figure 4) may produce an acidic nano-environment
271 (interface) contributing to grain dissolution and the release of additional Fe from the Pt-Fe alloy
272 surface (Guilbert 1986; Hattori et al. 2010). Hattori et al.'s (2010) suggestion that the surface of
273 the weathered Pt-Fe grains they studied consisted of a physical mixture of relict Pt-Fe alloy and
274 newly precipitated Fe3+-O-OH is corroborated with imaging and chemical analysis using FEG-
275 SEM; see Figures 4 and 5). Based on the detailed spectral analysis by Hattori et al. (2010), our
276 Fe *K*-edge absorption spectrum, with a larger peak at 7122 eV vs. 72128 eV suggests that only
277 trace iron exists on the surface of these Pt-Fe alloys, i.e., less weathering is occurring in the arid
278 Australian environment vs. New Caledonia.

279 Similar to gold (Reith et al., 2007; Southam et al., 2009), we see evidence for both
280 dissolution and re-precipitation occurring on individual Pt-Fe alloy grains. In Au-Ag systems,
281 Ag is leached and gold dissolution re-precipitation results in the formation of octahedral gold.
282 For Pt-Fe alloys, the leaching and oxidation of iron may contribute to the dissolution-re-
283 precipitation of Pt (see Traoré et al. 2008), resulting in occurrence of nanophase and
284 microcrystalline secondary aggregates of Pt (Figure 6 bc) revealed using EBSD analysis (Figure
285 7). Pt-Fe alloys may respond in the same manner as Au-Ag alloys, where the enrichment of Pt
286 (or Au) at the surface of these grains (respectively) may relate to the preferentially leaching, i.e.,
287 higher solubility of Fe (and Ag; Groen et al., 1990).

288 A model for near surface transformation of Pt, i.e., the dissolution, transportation and
289 precipitation of Pt, in soils and weathering profiles (Anthony and Williams 1994; Cabral et al.
290 2011) must continue to be developed to better understand placer Pt formation (see Fuchs and

Rose 1974; Bowles 1986; Azaroual et al. 2001; Bowles et al. 2004; Cabri et al. 1996; Hanley 2005; Reith et al. 2009; Cabral et al. 2011) and the mobility of Pt in Earth surface environments.

Implications

The physico-chemical extraction of intact, cubic Pt-Cu minerals from the surface of one, Pt-Fe alloy grain, and the development of secondary microcrystalline Pt at the surface of other Pt grains represent a strong case for the occurrence of nanophase Pt minerals in soils at Fifield. The dissolution and precipitation of secondary Pt also demonstrates that Pt is chemically mobile in surface weathering environments. The transport of these materials through gravity movement of soils, fluvial movement of sediment, and solution transport in water, will create a geochemical halo 'downgradient' from surface and near-surface Pt deposits. Methods development, targeting the recovery and quantification of these microscopic materials and/or soluble compounds from soils and sediments will increase the likelihood of detecting geochemical anomalies of Pt, which can serve as a means to vector in on Pt-deposits.

Acknowledgements

Electron Microscopy was performed in the Nanofabrication and ZAPLab imaging facilities (University of Western Ontario) and the AMMRF facility (University of Adelaide). Synchrotron analyses were conducted at the APS and ESRF. PNC/XSD facilities at the Advanced Photon Source, and research at these facilities, are supported by the US Department of Energy - Basic Energy Sciences, the Canadian Light Source and its funding partners, the University of Washington, and the Advanced Photon Source. Use of the Advanced Photon Source, an Office of Science User Facility operated for the U.S. Department of Energy (DOE)

Office of Science by Argonne National Laboratory, was supported by the U.S. DOE under Contract No. DE-AC02-06CH11357. We thank C. Plumridge, J. Kaminiski and the Rimfire Ltd. Pty. team for provision of samples and field support. Funding was provided by an Australian Research Council Discovery Grant DP20106946 to Reith, a Canadian NSERC Discovery Grant to Southam and the Australian Synchrotron Research Program.

References Cited

Anthony, E.Y., and Williams, P.A. (1994) Thiosulfate complexing of platinum group elements: Implications for supergene chemistry, In C.N. Alpers, and D.W. Bowles, Eds., American Chemical Society - Environmental Geochemistry of Sulfide Oxidation, pp. 551-560. ACS Books, Washington, DC.

Azaroual, M., Romand, B., Freyssinet, P., and Disnar, J. (2001) Solubility of platinum in aqueous solutions at 25°C and pHs 4 to 10 under oxidizing conditions. Geochimica et Cosmochimca Acta, 65, 4453-4466.

Barkov, A.Y., Fleet, M.E., Nixon, G.T., and Levson, V.M. (2005) Platinum-group minerals from five placer deposits in British Columbia, Canada. The Canadian Mineralogist, 43, 1687-1710.

Bowles, J.F.W. (1986) The development of platinum-group minerals in laterites. Economic Geology, 81, 1278-1285.

Bowles, J.F.W., Gize, A.P., and Cowden, A. (1994) The mobility of the platinum-group elements in the soils of the Freetown Peninsula, Sierra Leone. The Canadian Mineralogist, 32, 957-967.

Brugger, J., Etschmann, B., Grosse, C., Plumridge, C., Kaminski, J., Paterson, D., Shar, S.S., Ta, C., Howard, D.L., de Jonge, M.D., Ball, A.S., and Reith, F. (2013) Can biological toxicity drive the contrasting behavior of platinum and gold in surface environments? Chemical Geology, 343, 99-110.

Cabral, A.R., Beaudoin, G., Choquette, M., Lehmann, B., and Polonia, J.C. (2007) Supergene leaching and formation of platinum in alluvium: Evidence from Serro, Minas Gerais, Brazil. Mineralogy and Petrology 90, 141-150.

Cabral, A.R., Galbiatti, H.F., Kwitko-Ribeiro, R., and Lehmann, B. (2008) Platinum enrichment at low temperatures and related microstructures, with examples of hongshiite (PtCu) and empirical 'Pt_2HgSe_3' from Itabira, Minas Gerais, Brazil. Terra Nova, 20, 32-37.

Cabral, A.R., Radtke, M., Munnik, F., Lehmann, B., Reinholz, U., Riesemeier, H., Tupinambá, M., and Kwitko-Ribeiro, R. (2011) Iodine in alluvial platinum–palladium nuggets: Evidence for biogenic precious-metal fixation. Chemical Geology, 281, 125-132.

Cabri, L.J., Harris, D.C., Weiser, T.W. (1996) Mineralogy and distribution of platinum-group mineral (PGM) placer deposits of the world. Exploration and Mining Geology, 5, 73-167.

Cousins CA (1973) Platinoids of the Witwatersrand system. Journal of the South African Institute of Mining and Metallurgy, 73, 184-199.

Cousins, C.A., and Kinloch, E.D. (1976) Some observations on textures and inclusions in alluvial platinoids. Economic Geology, 71, 1377-1398.

Crawford, A.J., Meffre, S., Squire, R.J., Barron, L.M., and Falloon, T.J. (2007) Middle and Late Ordovician magmatic evolution of the Macquarie Arc, Lachlan Orogen, New South Wales. Australian Journal of Earth Sciences, 54, 181-214.

358 Dockrey, J.W., Lindsay, M.B.J., Mayer, K.U. Beckie, R.D. Norland, K.L.I Warren, L.A. and
359 Southam, G. (2014) Acidic microenvironments in waste rock characterized by neutral
360 drainage: Bacteria-mineral interactions at sulfide surfaces. Minerals, 4, 170-190.
361 Fairbrother, L., Brugger, J., Shapter, J., Laird, J.S., Southam, G., and Reith F. (2012) Supergene
362 gold transformation: Biogenic secondary and nano-particulate gold from arid Australia.
363 Chemical Geology, 320-321, 17-31.
364 Freyssinet, PH., Butt, C.R.M., Morris, R.C., and Piantone, P. (2005) Ore forming processes
365 related to lateritic weathering. Economic Geology, 100, 681-722.
366 Fuchs, W.A., and Rose, A.W. (1974) The geochemical behavior of platinum and palladium in
367 the weathering cycle in the Stillwater Complex, Montana. Economic Geology, 69, 332-
368 346.
369 Gornostayev, S.S., Crocket, J.H., Mochalov, A.G., Laajoki, K.V.O. (1999) The platinum-group
370 minerals of the Baimka placer deposits, Aluchin Horst, Russian Far East. The Canadian
371 Mineralogist, 37, 1117-1129.
372 Groen, J.C., Craig, J.R., Rimstidt, J.D. (1990) Gold-rich rim formation on electrum grains in
373 placers. The Canadian Mineralogist, 28, 207-228.
374 Guilbert, J.M. (1986) The geology of ore deposits, 985 p. W.H. Freeman and Company, New
375 York.
376 Hanley, J.J. (2005) The aqueous geochemistry of the platinum-group elements (PGE) in surficial,
377 low-T hydrothermal and high-T magmatic-hydrothermal environments. In J.E. Mungall
378 Ed., Exploration for Platinum-group Element Deposits - Mineralogical Association of
379 Canada Short Course Series Volume 35, p. 35-56. Mineralogical Association of Canada,.
380 Ottawa, Canada.

Hattori, K.H., Takahashi, Y., Augé, T. (2010) Mineralogy and origin of oxygen-bearing platinum-iron grains based on an X-ray absorption spectroscopy study. American Mineralogist, 95, 622-630.

Johan, Z., Ohnenstetter, M., Slansky, E., Barron, L.M., Suppel, D. (1989) Platinum mineralization in the Alaskan-type intrusive complexes near Fifield, New South Wales, Australia Part 1: Platinum-group minerals in the clinopyroxenites of the Kelvin Grove Prospect, Owendale Intrusion. Mineralogy and Petrology, 40, 289-309.

Koek, M., Kreuzer, O.P., Maier, W.D., Porwal, A.K., Thompson, M., and Guj, P. (2010) A review of the PGM industry, deposit models and exploration practices: Implications for Australia's PGM potential. Resources Policy, 35, 20-35.

Kortright, J.B., and Thompson, A.C. (2001) X-ray emission energies. In A.C. Thompson, and D. Vaughan, Eds. X-ray Data Booklet, Section 1.2. Lawrence Berkeley National Laboratory, University of California, Berkeley, California.

Kwitko, R., Cabral, A.R., Lehmann, B., Laflamme, J.H.G., Cabri, L.J., Criddle, A.J., and Galbiatti, H.F. (2002) Hongshiite (PtCu) from itibirite-hosted Au-Pd-Pt mineralization (Jacutinga), Itabira district, Minas Gerais, Brazil. The Canadian Mineralogist, 40, 711-723.

MacDonald, A.J. (1987) Ore deposit models #12: The platinum group element deposits-classification and genesis. Geoscience Canada, 14, 155-166.

Melcher, F., Oberthu□r, T., and Lodziak, J. (2005) Modification of detrital platinum-group minerals from the eastern Bushveld complex, South Africa. The Canadian Mineralogist, 43, 1711-1734.

403 Northcote, K.H. (1979) A factual key for the recognition of Australian soils. 4th Edition, Rellim
404 Technical Publications, Glenside, Australia.
405 Oberthu□r, T. (2002) Platinum-group element mineralization of the Great Dyke, Zimbabwe. In
406 L.J. Cabri. Ed., The Geology, Geochemistry, Mineralogy and Mineral Beneficiation of
407 Platinum-Group Elements Special Volume, Canadian Institute of Mining, Metallurgy and
408 Petroleum, 54, 483-506.
409 Oberthu□r, T., Weiser, T.W., and Gast, L. (2003) Geochemistry and mineralogy of platinum-
410 group elements at Hartley Platinum Mine, Zimbabwe. Part 2: Supergene redistribution in
411 the oxidized Main Sulfide Zone of the Great Dyke, and alluvial platinum-group minerals.
412 Mineralium Deposita, 38, 344-355.
413 Oberthu□r, T., Melcher, F., Gast, L., Wöhrl, C., and Lodziak, J. (2004) Detrital platinum-group
414 minerals in rivers draining the eastern Bushveld complex, South Africa. The Canadian
415 Mineralogist, 42, 563-582.
416 Oberthu□r, T., Weiser, T.W., Melcher, F., Gast, L., and Woehrl, C. (2013) Detrital platinum-
417 group minerals in rivers draining the Great Dyke, Zimbabwe. The Canadian Mineralogist,
418 51, 197-222.
419 O'Day, P.A., Rivera, N., Root, R., and Carroll, S.A. (2004) X-ray absorption spectroscopic study
420 of Fe reference compounds for the analysis of natural sediments. American Mineralogist,
421 89, 572-585.
422 Ottemann, J., and Augustithis, S. (1967) Geochemistry and origin of "platinum-nuggets" in
423 lateritic covers from ultrabasic rocks and birbirites of W. Ethiopia. Mineralium Deposita,
424 1, 269-277.

425 Ravel, B., and Newville, M., 2005. ATHENA, ARTEMIS, HEPHAESTUS: data analysis for X-
426 ray absorption spectroscopy using IFEFFIT. Journal of Synchrotron Radiation, 12, 537-
427 541.

428 Reith, F., Lengke, M.F., Falconer, D., Craw, D., and Southam, G. (2007) The geomicrobiology
429 of gold. International Society for Microbial Ecology Journal, 1, 567-584.

430 Reith, F., Etschmann, B., Grosse, C., Moors, H., Benotmane, M.A., Monsieurs, P., Grass, G.,
431 Doonan, C., Vogt, S., Lai, B., Martinez-Criado, G., George, G.N., Nies, D.H., Mergeay,
432 M., Pring, A., Southam, G. and Brugger, J. (2009) Mechanisms of gold biomineralization
433 in the bacterium *Cupriavidus metallidurans*. Proceeding of the National Academy of
434 Sciences, 106, 17757-17762.

435 Reith, F., Fairbrother, L., Nolze, G., Wilhelm, O., Clode, P.L., Gregg, A., Parsons, J., Wakelin,
436 S., Pring, A., Hough, R., Southam, G., and Brugger, J. (2010) Nanoparticle factories:
437 Biofilms hold the key to gold dispersion and nugget formation. Geology, 38, 843-846.

438 Ryan, C.G., Etschmann, B.E., Vogt, S., Maser, J., Harland, C., van Achterbergh, E., and Legnini,
439 D. (2005) Nuclear Microprobe – Synchrotron Synergy: Towards Integrated Quantitative
440 Real-time Elemental Imaging using PIXE and SXRF. Proceedings of the ICNMTA'2004
441 conference. Nuclear Instruments and Methods B 231, 183-188.

442 Ryan, C.G., Siddons, D.P., Moorhead, G., Kirkham, R., De Geronimo, G., Etschmann, B.E.,
443 Dragone, A., Dunn, P.A., Kuczewski, A., Davey, P., Jensen, M., Ablett, J.M.,
444 Kuczewski, J., Hough, R., and Paterson, D. (2009) High-throughput X-ray fluorescence
445 imaging using a massively parallel detector array, integrated scanning and real-time
446 spectral deconvolution. Journal of Physics: Conference Series 186, 012013,
447 doi:10.1088/1742-6596/186/1/012013.

448 Ryan, C.G. (2000) Quantitative Trace Element Imaging using PIXE and the Nuclear Microprobe.
449 International Journal of Imaging Systems and Technology, 11, 219-230.
450 Schneiderhöhn, H., and Moritz, H. (1939) Die oxydationszone im platinfu□hrenden
451 sulfidpyroxenit (Merensky Reef) des Bushvelds in Transvaal. Zentralblatt fu□r
452 Mineralogie, Geologie und Paläontologie A, 1-12.
453 Sillitoe, R. (2005) Supergene oxidized and enriched porphyry copper and related deposits.
454 Economic Geology, 100, 723-768.
455 Slansky, E., Johan, Z., Ohnenstetter, M., Barron, L.M., and Suppel, D. (1991) Platinum
456 mineralization in the Alaskan-type intrusive complexes near Fifield, N.S.W., Australia.
457 Part 2. Platinum-group minerals in placer deposits at Fifield. Mineralogy and Petrology,
458 43, 161-180.
459 Southam, G., Lengke, M.F., Fairbrother, L., and Reith, F. (2009) The biogeochemistry of gold.
460 Elements, 5, 303-307.
461 Suárez, S., Prichard, H.M., Velasco, F., Fisher, P.C., and McDonald, I. (2008) Weathering of the
462 platinum group minerals in the Aguablanca Ni-Cu Gossan (SW Spain). Revista de la
463 Sociedad Española de Mineralogía, 9, 237-238.
464 Teluk, A.J. (2001) Fifield Platinum Project, NSW, Australia: Geodyne Pty Ltd Technical Report
465 (electronic copy available from <http://www.rimfire.com.au/
466 PDF/Geodynereportcompletewithfigs.pdf.> last accessed on 30 March 2012), 71 p.
467 Traoré, D., Beauvais, A., Auge, T., Parisot, J.C., Colin, F., and Cathelineau, M. (2008) Chemical
468 and physical transfers in an ultramafic rock weathering profile: Part 2- Dissolution vs.
469 accumulation of platinum group minerals. American Mineralogist, 93, 31-38.

Weiser, T.W. (2002) Platinum-group minerals (PGM) in placer deposits. In L.J. Cabri, Ed., The Geology, Geochemistry, Mineralogy, and Mineral Beneficiation of Platinum-Group Elements. Canadian Institute of Mining, Metallurgy, and Petroleum, Special Volume 54, 721-756.

Williams, G.P. (2001) Electron binding energies. In A.C. Thompson, and D. Vaughan, , Eds., X-ray Data Booklet, Section 1.1. Lawrence Berkeley National Laboratory, University of California, Berkeley, California.

List of Figure Captions

Figure 1. Map of Australia with Fifield study site indicated by a circle in state of New South Wales.

Figure 2. Dominant Pt-Fe alloy morphologies occurring in sample of grains collected at the from Fifield Platina Deep Lead, NSW, Australia: (**a**) anhedral grain, with dissolution channels; (**b**) knobby grain with remnants of minerals and negative imprints of crystals; (**c**) platy subhedral grain with abundant coatings of red-brown Fe-hydroxides; (**d**) anhedral grain coated by orange-red Fe-hydroxides; (**e**) smooth well-rounded apparently alluvially worn, grain with polished surface; (**f**) anhedral grain with highly transformed surface.

Figure 3. (**a-d**) A representative series of electron microprobe maps showing the distribution of Pt (max. 86.7 wt. %), Fe (max. = 21.9 wt. %), Ir (max. 54.9 wt. %) and Os (max. 32.3 wt. %) in a rounded Pt-Fe alloy grain from Fifield, New South Wales Australia.

Figure 4. (**a-c**) A SEM micrograph focal series of weathered Pt-Fe alloy; note the ca. 150 nm cubic minerals in panel **c**. (**d and e)** Fe and Cu element maps of grain, respectively. Color scales in **d** and **e** show relative element concentrations and transition upward from low concentration (black) to high concentration (white). Note the rectangular area in **e**, which shows a streak of copper that corresponds to the Cu-rich cubic minerals observed in panel **b**. **(f)** SEM micrograph of cubic 'pits' and EDS spectra comparing the elemental composition of the bulk grain and cubic mineral rich areas. The bulk grain is Pt-Fe alloy (with trace Cu and Rh) while the cubic minerals show elevated Cu. (**g**) SEM and EDS of the acicular, Fe-hydroxides with co-precipitated trace Ce and Rh.

Figure 5. (**a**) SEM micrographs of sub-rounded Pt-Fe alloy; note dented and scratched surface, in-filled with clay and organics-darker grey coating); (**b**) a deeply pitted sub-rounded Pt-Fe alloy with relatively deep circular pits in-filled with secondary minerals; (**c** and **d**) micrographs of Pt-Fe alloy coated with acicular, Fe-hydroxides. (**e**) EDXA spectrum of the acicular Fe hydroxides indicates that cerium and rhodium is present in these samples. (**f**) experimental XANES spectrum and standard spectra for oxidized Fe-species demonstrating that the iron rich coating is comprised of Fe-oxides, intuitively iron hydroxide based on the rust-coloration on the grain.

Figure 6. (**a** and **b**) Low and high magnification BSE-SEM micrographs of a weathered Pt-Fe alloy focusing on the grain surface, highlighting the presence of sub-micrometer-scale Pt. (**c**) SEM of aggregate, native Pt consisting of Pt-platelets within an organic film on the surface of Pt-Fe alloy; (**d**) SEM micrograph of a FIB-milled Pt-fe alloy showing increasing native Pt crystal size as you get closer to the rim; (**e** and **f**) high magnification SEM micrographs of the rim of the

516 FIB-milled grain showing an increased number of grain boundaries, indicating the formation of
517 microcrystalline native Pt at the .Pt-Fe alloy surface.
518
519 **Figure 7.** (**a**) SEM micrograph of a FIB-sectioned Pt-Fe alloy with EBSD map showing the
520 twinned crystal orientation of the grain-center overlain; (**b**) detailed SEM micrographs and
521 EBSD map of the grain rim showing micro-crystalline secondary Pt; (**c**) Synchrotron μXRF map
522 of Pt, Fe and Os (Red, Green, Blue), respectively, (**d-f**) showing the differences in Pt and Fe
523 from the center of the grain towards the rim; μXRF map of Pt (max. 90.6 wt. %); μXRF map of
524 Fe (max. 16.8 wt. %); μXRF map of Os (max. 6.4 wt. %).

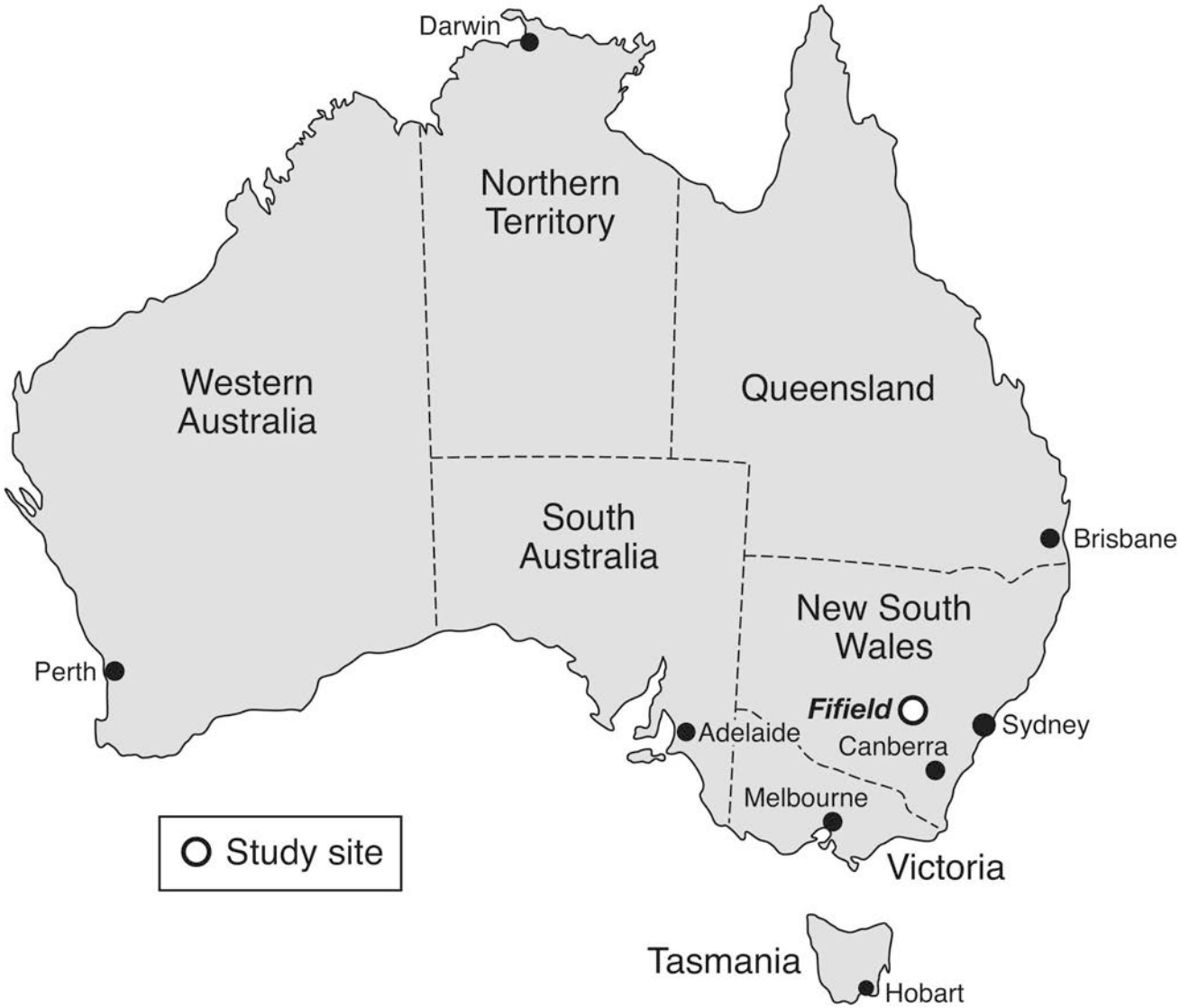
Darwin
Northern Territory
Western Australia
Queensland
South Australia
Brisbane
New South Wales
Perth
Fifield
Adelaide
Canberra
Sydney
Melbourne
Victoria
Study site
Tasmania
Hobart

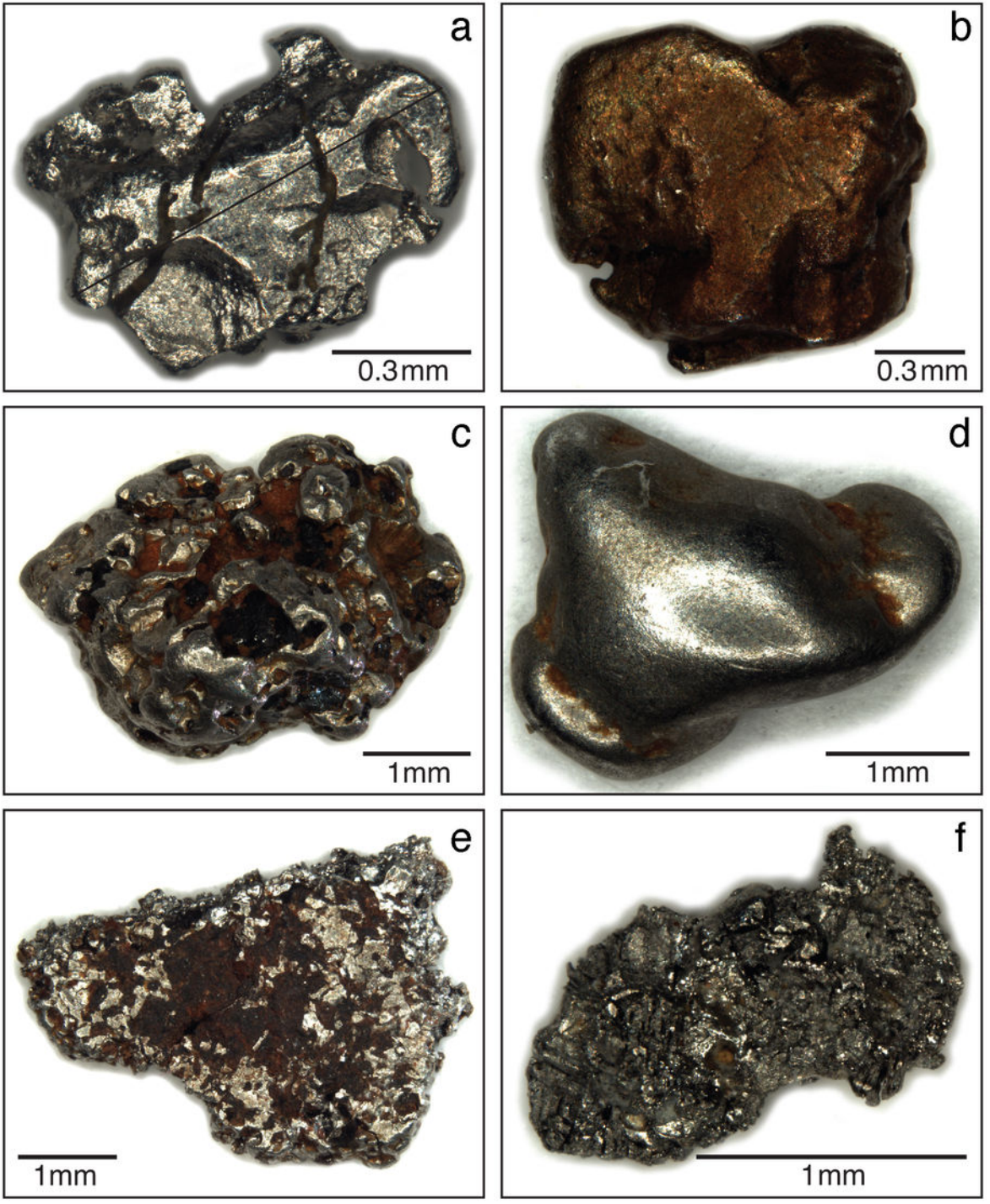
a
0.3mm
b
0.3mm
c
1mm
d
1mm
e
1mm
f
1mm

a

Pt

1mm

b

Fe

1mm

c

Ir

1mm

d

Os

1mm

MIN

MAX

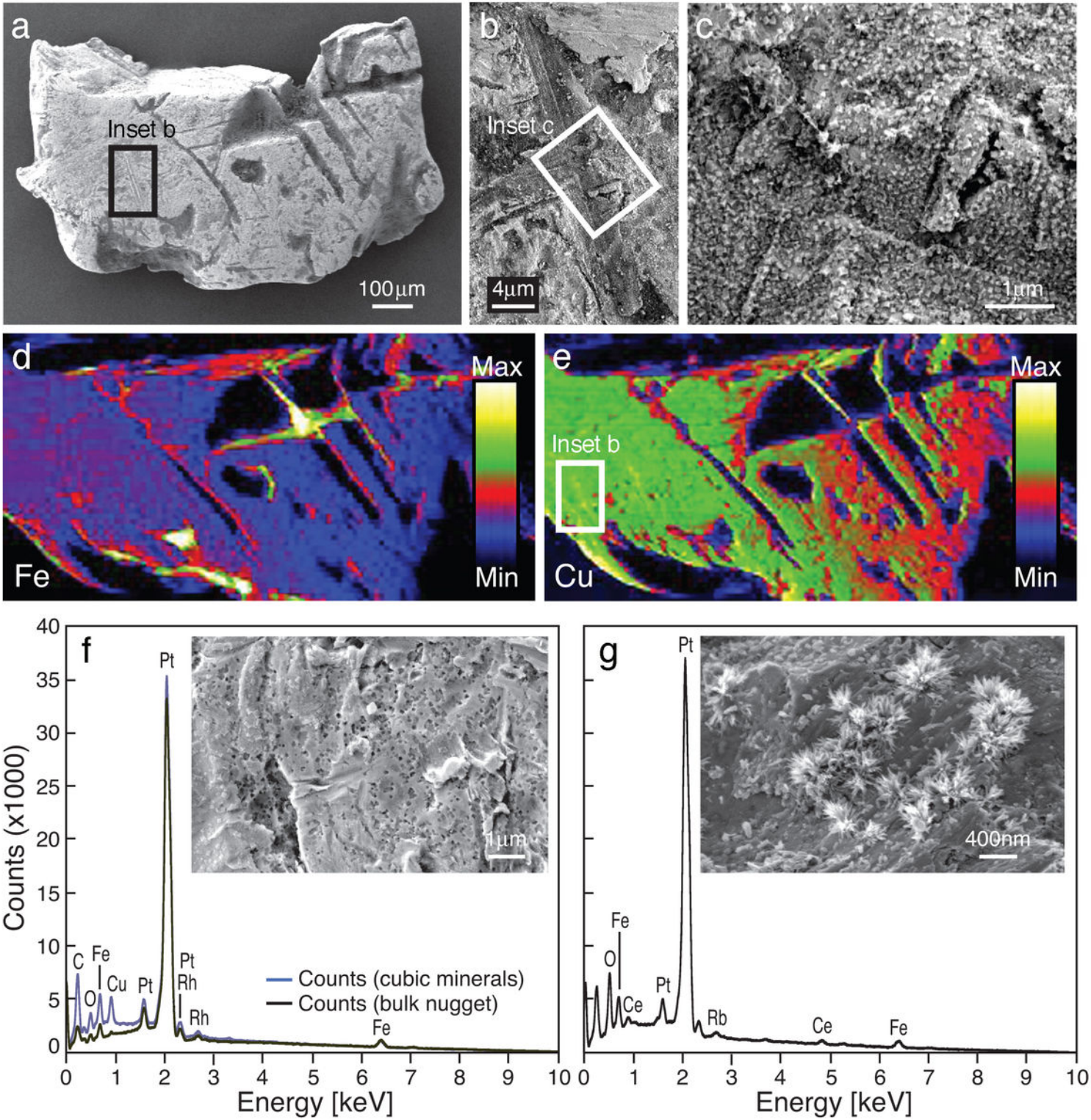
a
Inset b
100µm
b
Inset c
4µm
c
1µm
d
Max
Min
Fe
e
Inset b
Max
Min
Cu
f
Pt
1µm
C
Fe
O
Cu
Pt
Pt
Rh
Rh
Fe
Counts (cubic minerals)
Counts (bulk nugget)
Counts (x1000)
Energy [keV]
g
Pt
400nm
Fe
O
Ce
Pt
Rb
Ce
Fe
Energy [keV]

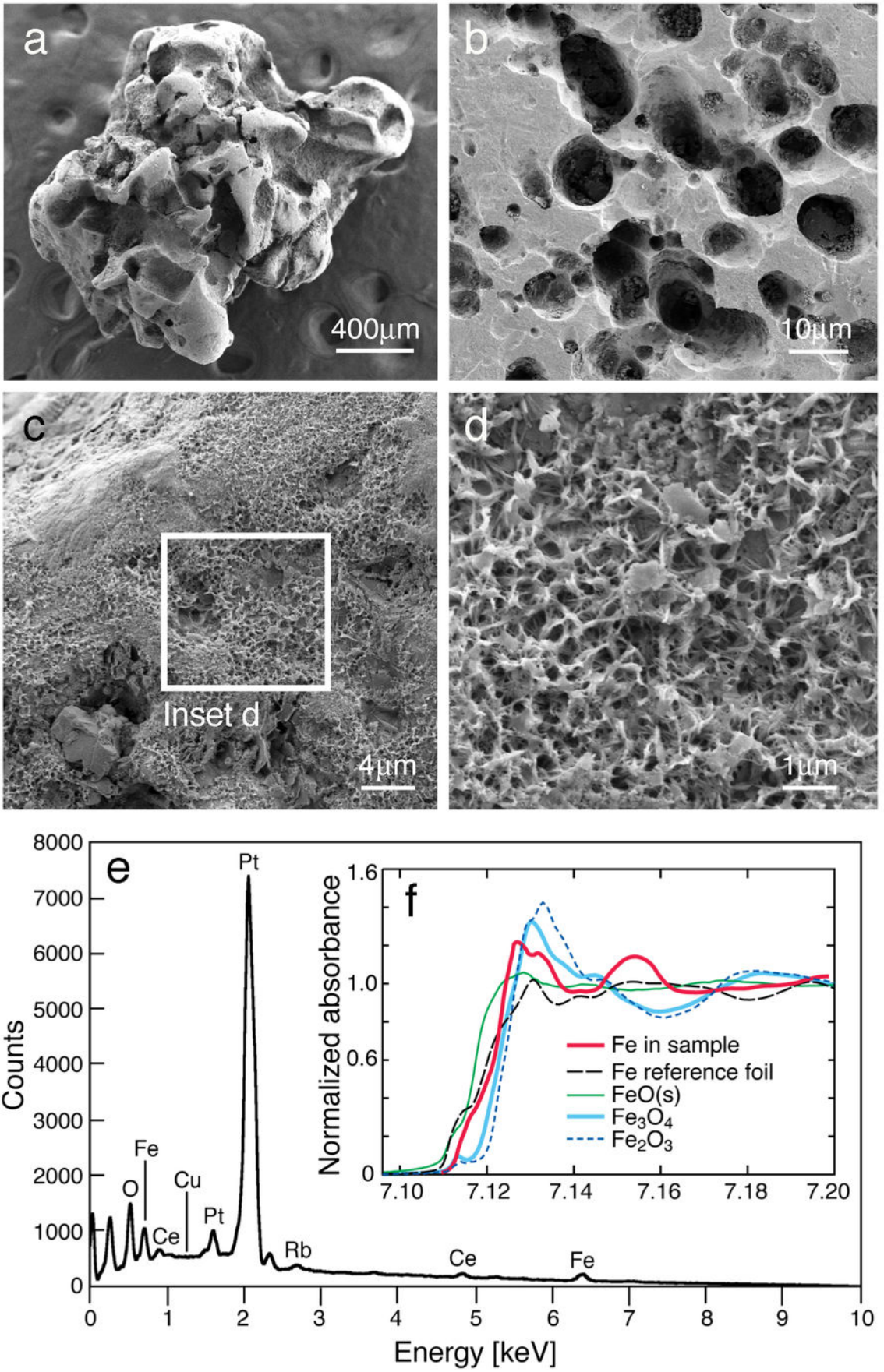
a
400µm
b
10µm
c
Inset d
4µm
d
1µm
e
Counts
Energy [keV]
O
Fe
Ce
Cu
Pt
Pt
Rb
Ce
Fe
f
Normalized absorbance
Fe in sample
Fe reference foil
FeO(s)
Fe3O4
Fe2O3

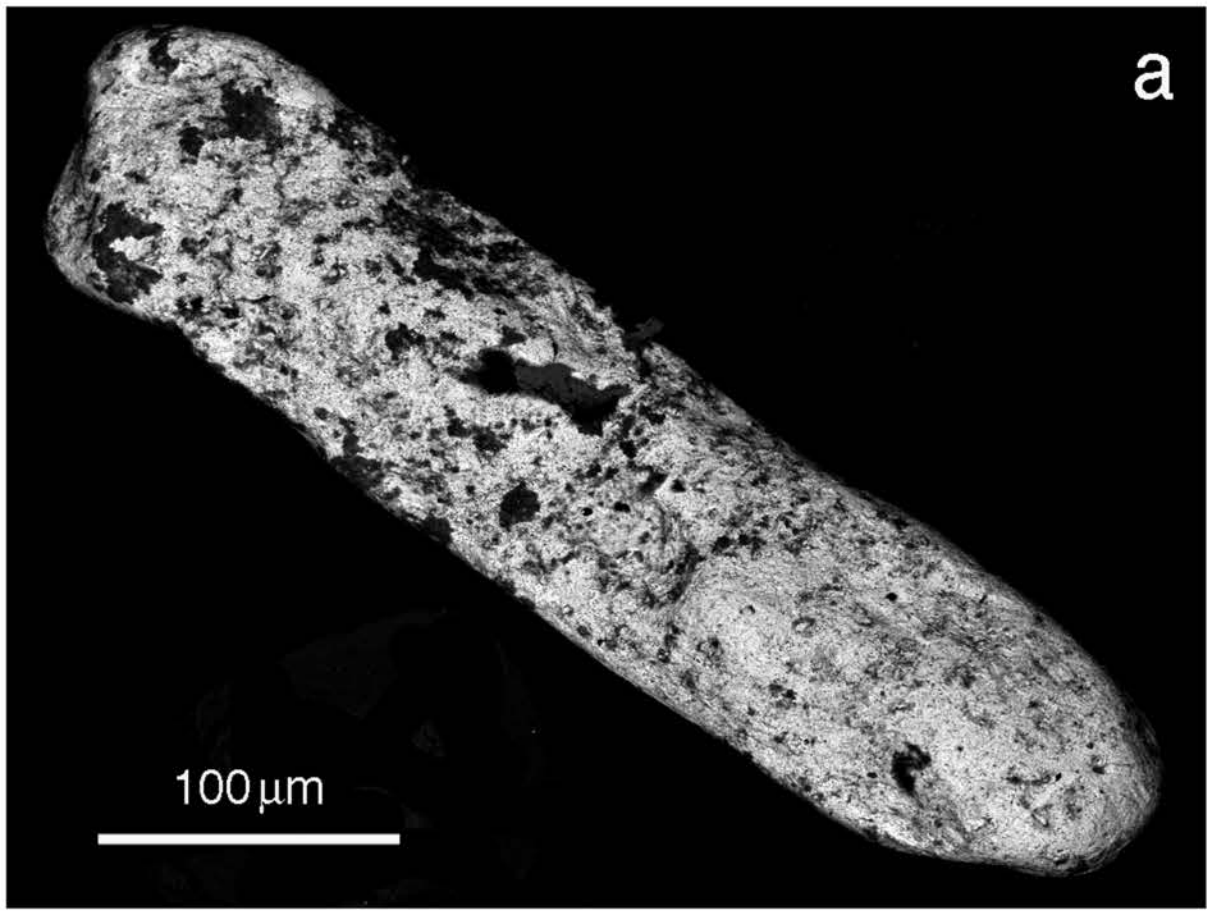
a
100 µm

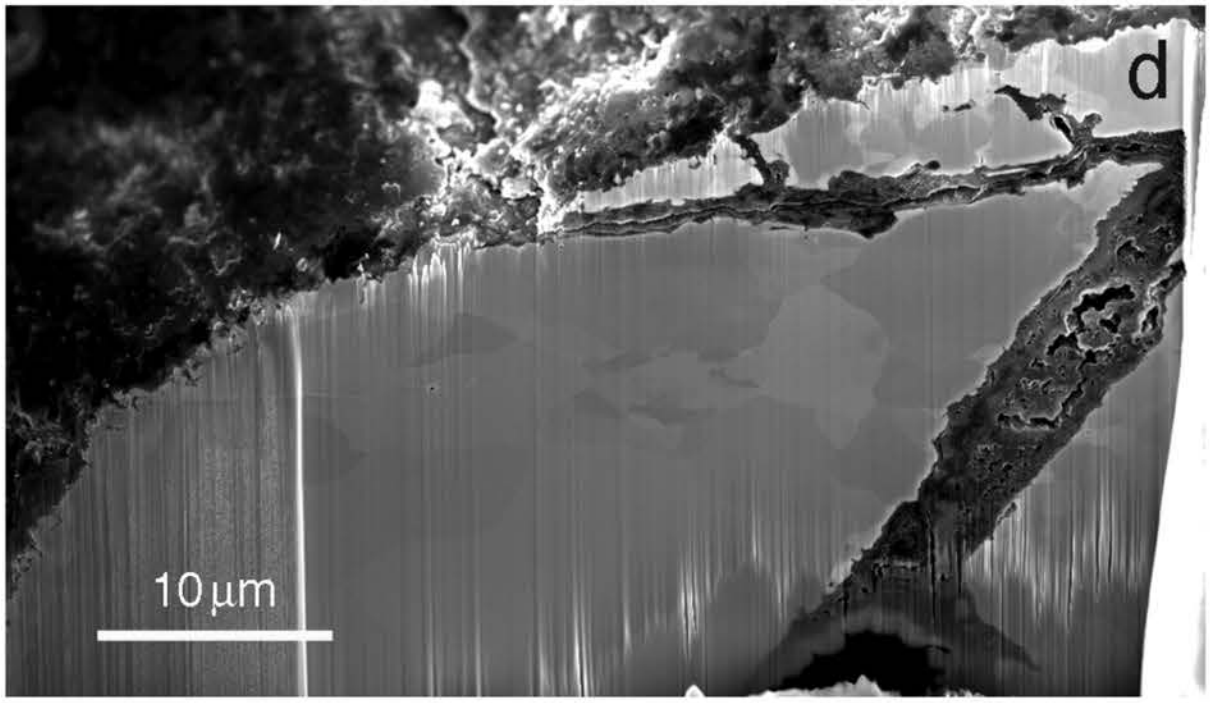
d
10 µm

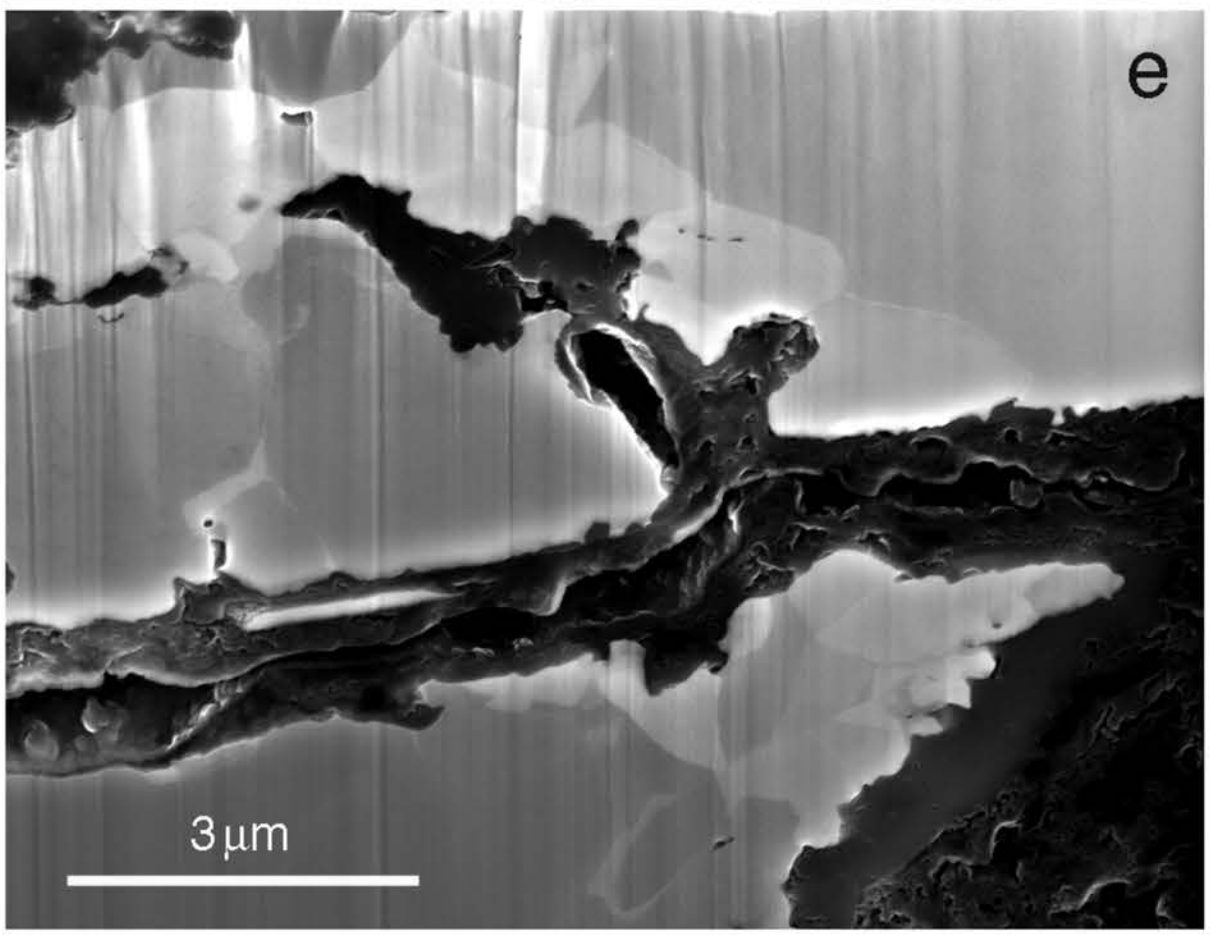
e
3 µm

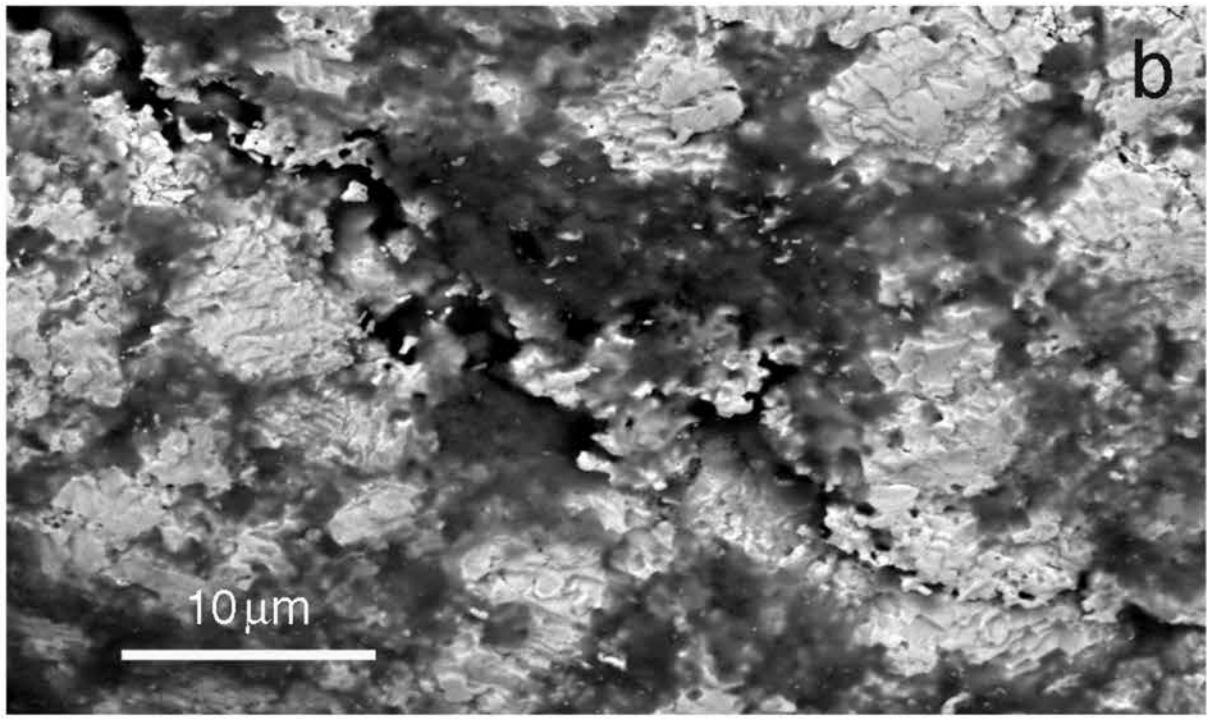
b
10 µm

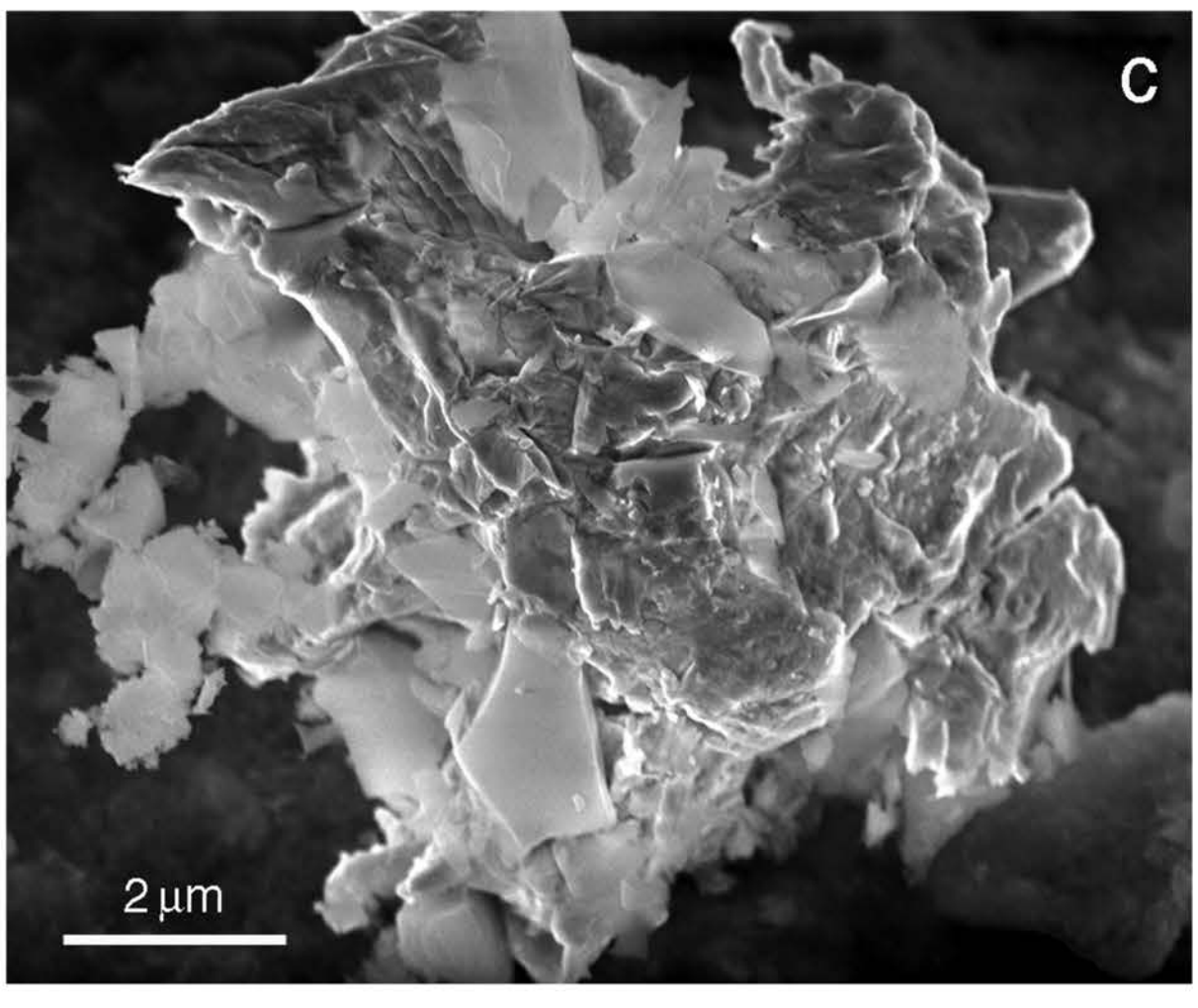
c
2 µm

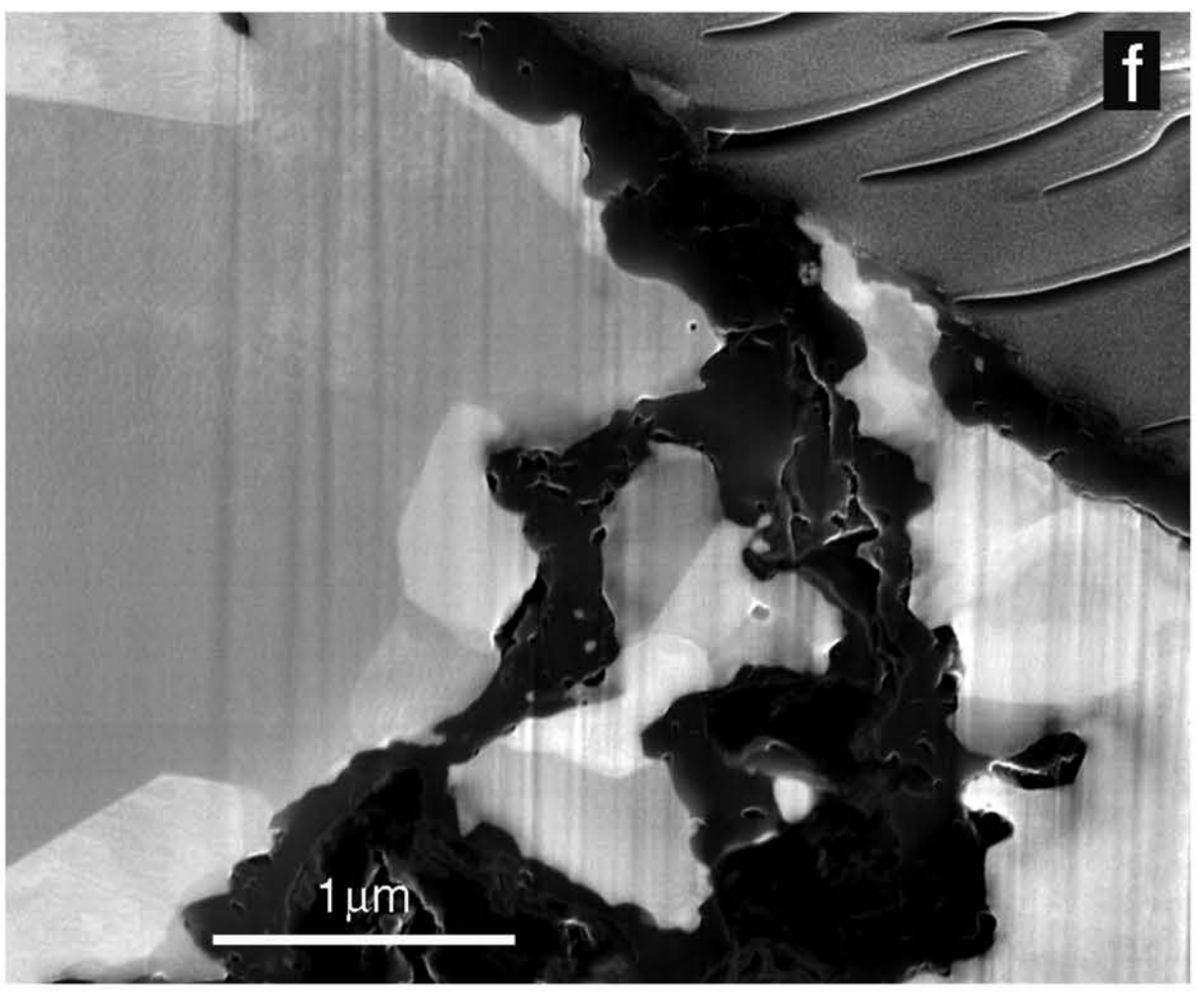
f
1 µm

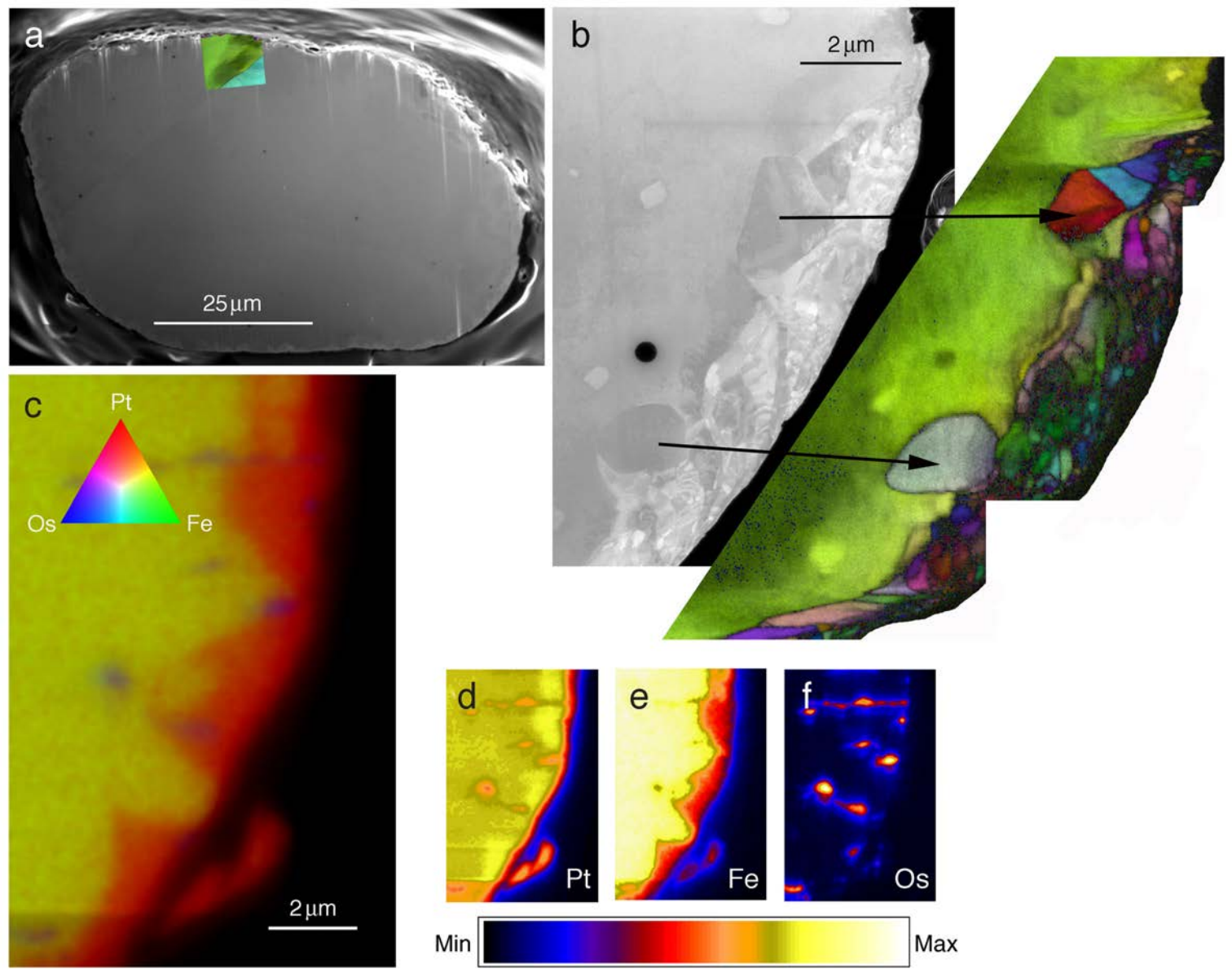
a
25 µm
b
2 µm
c
Pt
Os
Fe
2 µm
d
Pt
e
Fe
f
Os
Min
Max